ChemComm

Accepted Manuscript

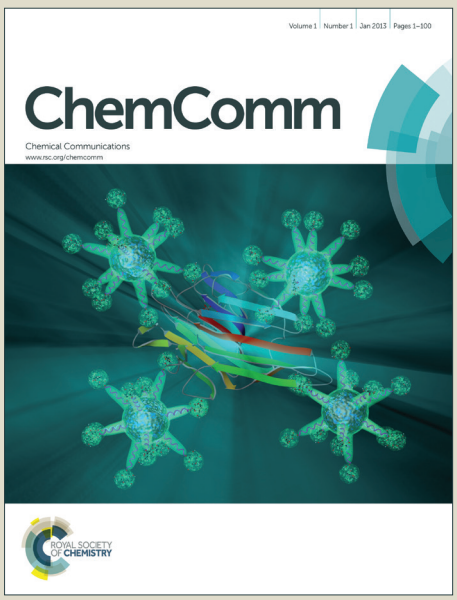

ROYAL SOCIETY OF CHEMISTRY

www.rsc.org/chemcomm

Journal Name

RSCPublishing

COMMUNICATION

Gas Storage and Separation in Water-Stable $[Cu^{I}_{5}BTT_{3}]^{4-}$ Anion Framework Comprising Giant Multi-prismatic Nanoscale Cage

Cite this: DOI: 10.1039/x0xx00000x

Received 00th January 2012,
Accepted 00th January 2012

DOI: 10.1039/x0xx00000x

www.rsc.org/

B. X. Dong,*[a] S. Y. Zhang,[a] W. L. Liu,[a] Y. C. Wu,[a] J. Ge,[a] L. Song[a] and Y. L. Teng*[a]

A novel water-stable open poly-nuclear Cu(I)-based metal-organic framework, $[NC_2H_8]_4Cu_5(BTT)_3 \cdot xG$ (G=guest of DMA and H_2O) (1), featuring with giant multi-prismatic nanoscale cage, and high CO_2/N_2 and CO_2/H_2 sorption selectivities, was successfully assembled by using the nitrogen-rich ligand of 1,3,5-tris(2H-tetrazol-5-yl)benzene (H_3BTT) to bridge two types of Cu_3 and Cu_2 clusters.

With CO_2 being one of the greatest contributors to global warming (ca. 30 Gt per year of worldwide CO_2 emissions), there is increasing interest in removing CO_2 from the air to combat the greenhouse gas effect.[1] The development of carbon capture and sequestration (CCS) technologies that efficiently capture CO_2 from existing emission sources is of critial importance to the current energy framework, since the transition of the existing infrastructure from carbon-based sources to cleaner alternatives requires considerable modifications to be realized.[2] The key process in CCS is the capture of CO_2 from pre-combustion shifted syngas and post-combustion flue gas.[3] Pre-combustion CO_2 capture is a process in which fuel is decarbonated prior to combustion. It is especially used for the separation of CO_2 from H_2 within the mixture, which can then be performed to afford pure H_2 suitable for the generation of electricity in fuel cell industry.[4] The principle of post-combustion capture is to remove CO_2 from flue gas after combustion at low pressure and low-CO_2-content. For a typical post-combustion flue gas for a coal-fired power plant, N_2 (73–77%), CO_2 (15–16%), H_2O (5–7%) and O_2 (3–4%) are the main constituents. Chemical absorption of CO_2 using monoethanolamine is a leading technology in post-combustion capture which can efficiently remove CO_2 from the flue gas. However, large energy penalty is associated with the liberation of captured CO_2 from the capture medium. In contrast, physisorption process requires much less energy which could allow conveniently reversible process to capture CO_2 gas. Since the low concentration of CO_2 and large quantities of N_2 originating from the flue gas, the selectivity toward CO_2 is crucial for the adsorption-based separation processes.[2a,5] Therefore, high selectivity, moderate affinity of the materials toward CO_2, high stability and low cost as well as high adsorption uptake are the most important criteria by which new adsorbents for improving CO_2/N_2 or CO_2/H_2 separation performance will be judged for the CCS process concerning physical absorption technology.[5]

In the past few decades, extensive research efforts have been mainly focused on porous solids of zeolites[6] and activated carbons.[7] The common shortfalls of these traditional adsorbents are either low capacities or difficult regeneration processes. Porous metal-organic frameworks (MOFs), as a promising class of sorbents, have many properties that make them attractive for applications in gas storage, molecular recognition and separation, heterogeneous catalysis, and biomedical area.[8] In regard to CO_2/N_2 separation relevant to post-combustion CO_2 capture, to the best of our knowledge, a record of simulated selectivity (~1.9×10^4 for CO_2/N_2=15/75) was found in rho-ZMOF[9] and a record on the basis of experiment (1700 for CO_2/N_2=10/90, which was validated by gas mixture gravimetric adsorption experiments at various pressures) was found in SIFSIX-3-Zn by Zaworotko *et al*.[10] The top CO_2/N_2 selectivities (CO_2/N_2=15/75) at 298 K, on the basis of experiments, are ~165 in the post-synthesis modified mmen-Cu-BTTri,[11] ~101 in the HKUST-1 with coordinatively unsaturated metal sites,[12] ~65 in the bio-MOF-11 with multiple Lewis basic sites afforded by adenine,[3] and ~45 in the zinc-paddle wheel MOF with highly polar ligands.[13] A remarkable enhancement of the CO_2/N_2 selectivity was achieved through axial ligand substitution of Cl^- by TiF_6^{2-}.[14] Research on MOFs aiming for the separation of CO_2 from H_2 are still in their infancy although significant promise in this regard is offered by them.[3,4,15] Two frameworks with exposed metal cation sites, $H_3[(Cu_4Cl)_3(BTTri)_8]$ (CuBTTri) and Mg_2(dobdc) display by far the highest selectivities of CO_2/H_2, probably owing to the greater polarizability of CO_2 versus H_2.[4]

To develop new MOFs sorbents for CO_2 capture, a new route is the design and construction of open MOFs through the incorporation of accessible nitrogen-donor groups, such as pridine, imidazole, triazole and tetrazole, into the pore walls of porous materials which can dramatically affect the gas uptake capacity and selectivity of the materials.[16] For example, compounds of CuBTTri[17] and NTU-105[18] incorporated with nitrogen-rich or coordination-free triazole units exhibit high stability and remarkable uptake towards CO_2 (14.3 wt% at 298 K and 90 wt% at 195 K for the former; 26.8 wt% at 273K for the latter). For this reason, we are especially interested in ligand containing multiple tetrazole group (1,3,5-tris(2H-tetrazol-5-yl)benzene or H_3BTT in short, see Fig. S1, ESI†), as such ligand can

achieve high connectivity and high percentage of open nitrogen-donor sites.

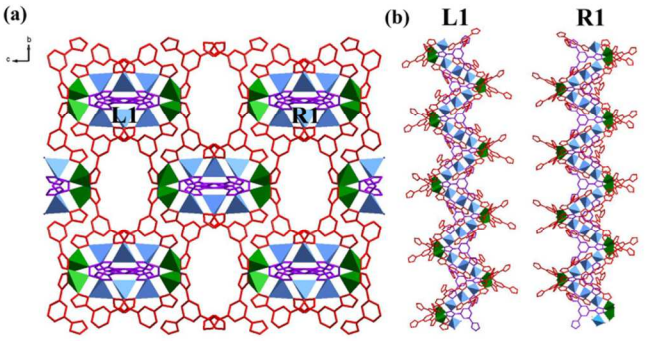

Fig. 1 (a) View of the 3D open anion framework of **1** embedded with meso-helical chains; (b) View of the L1 and R1 helical chains.

Reaction of $CuCl_2 \cdot 2H_2O$ (0.068 g, 0.4 mmol) and $H_3BTT \cdot 2HCl$ (0.071 g, 0.2 mmol) in DMA (*N,N′*-Dimethylacetamide) solvent at 140 °C for 3 days afforded $[NC_2H_8]_4Cu_5(BTT)_3 \cdot xG$ (G=guest of DMA and H_2O) (**1**) as brown microcrystalline powders. Single-crystal X-ray diffraction analysis reveals that **1** crystallizes in the orthorhombic *Fddd* space group. The asymmetric unit of the solvent-free structure contains four dimethylammonium cations, three crystallographically independent Cu^I centers, two BTT^{3-} ligands (BTT-1 and BTT-2), in which Cu(3) atom and BTT-1 molecule are half-occupied, as shown in Fig. S2, ESI†. The dimethylammonium cations are origining from the decomposition of the DMA molecule. All Cu^I centers are four-coordinated by four nitrogen atoms from four tetrazole rings in different BTT molecules in a distorted tetrahedral geometry. The Cu–N distances are in the range of 1.978(2)–2.097(2) Å. It should be noted that BTT-1 and BTT-2 exhibit different coordination styles, which serve as μ_{8}- and μ_{6}-bridgings, respectively, bonding to eight and six Cu^I centers, respectively (Fig. S3, ESI†). After careful examination of the structures, we found that three apical tetrazole rings and the central benzene ring are not coplanar in both BTT ligands, which show ca. 27.7, 20.5, 32.6º (in BTT-1) and ca. 40.7, 19.4, 19.4º (in BTT-2) for the dihedral angles between the phenyl ring and each of the tetrazole planes (Fig. S3, ESI†). Through the connection of BTT-2 and BTT-1, respectively, a Cu_3 cluster and a Cu_2 cluster are formed, which are further linked to form linear chains along *a* axis and *b* axis (Fig. S4, ESI†). The Cu_3 and Cu_2 clusters in the corresponding 1D chain are further terminally coordinated by BTT-1 and BTT-2 ligands, respectively, leading to a 3D open framework imparting meso-helical chains as viewed along [100] direction (Fig. 1a). The two symmetrically related helices (which are labled as L1 and R1) coexist and arrange alternatively in the centrosymmetric structure (Fig. 1b), which results in an achirality structure. The pitch for the helice, represented by the Cu3···Cu3 distance, is 14.62 Å.

A prominent structural feature of **1** is the presence of a giant multi-prismatic nanoscale cage built from the upholding of the helices, in which large cavities (23.8 Å × 18.9 Å × 16.2 Å, Fig. 2) are interconnected with four types of small windows (~6.4 Å × 10.4 Å, ~6.9 Å ×11.2 Å, ~8.8 Å × 10.3 Å and ~4.0 Å ×4.3 Å; see Fig. S5, ESI†). Extensive nitrogen-donor sites of 67% are exposed to the four types of channels which enable compound **1** to serve as promising porous material for gas storage and separation. The solvent-accessible void fraction calculated using PLATON[19] is ~40.5% of the total crystal volume (31702 $Å^3$).

PXRD patterns for the as-synthesized material and samples after treatment at different conditions are shown in Fig. S6 (ESI†). The diffraction peaks of the as-synthesized MOF match well with the simulated pattern on the basis of the single-crystal structure. Crystalline **1** is stable in air, DMA, methanol, acetone and water, as confirmed from the PXRD test. Thermogravimetric analyses (TGA) indicate that the acetone, as compared with methanol, is a better solvent for exchanging the higher boiling point solvents of DMA and water remained in **1** (Fig. S7, ESI†).

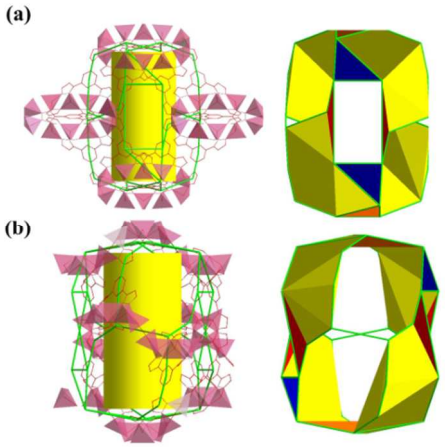

Fig. 2 View of the giant cavity and the 3D scheme from *a* (a) and *b* (b) axis.

In order to confirm its permanent porosity, N_2 sorption isotherm was collected at 77 K. An activated sample **1a** was prepared by exchange of the solvent of the as-synthesized **1** with acetone followed by evacuation at 40 ºC. The N_2 sorption isotherm (Fig. S8, ESI†) of **1a** shows typical Type I behaviour, indicating a microporous structure, with a Brunauer–Emmett–Teller (BET) surface area of 701 $m^2\ g^{-1}$ (Langmuir surface area of 801 $m^2\ g^{-1}$). The BET surface area was calculated from a line regression plot of $1/(Q(P_0/P–1)$ versus P_0/P, where Q is the total volume absorbed at a particular point P_0/P and P_0 is 1 atm pressure, within the range $0.005 < P_0/P < 0.05$ (Fig. S9, ESI†). The single point adsorption total pore volume at P = 0.99 bar from the N_2 sorption data is 0.302 $cm^3\ g^{-1}$, which is a little lower than the value of 0.36 $cm^3\ g^{-1}$ estimated from the single-crystal structure. The activated **1a** also reversibly adsorbs up to 1.03 wt% (116 $cm^3\ g^{-1}$) of hydrogen gas at 77 K and 1 bar (Fig. S8, ESI†), which is much less than those of M–BTT (M=Fe, Mn, Cu) series MOFs with exposed M^{2+} coordination sites (1.7–2.3 wt%, Table S5, ESI†).

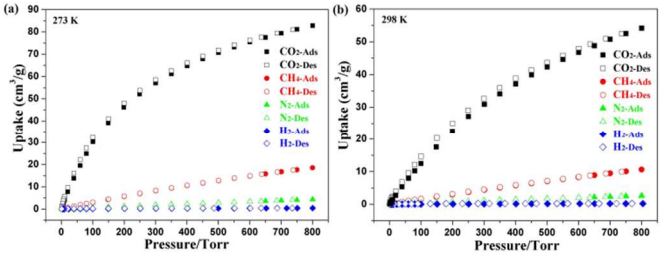

Fig. 3 Gas sorption isotherms of CO_2 (black square), CH_4 (red circle), N_2 (green triangle) and H_2 (blue diamond) for **1a** at 273 K (a) and 298 K (b).

Establishment of the permanent porosity of **1a** encourages us to examine its potential application of selective gas separation. Interestingly, **1a** has higher affinity and capacity for CO_2 (82.8 $cm^3\ g^{-1}$, 3.7 mmol g^{-1} and 14.0 wt% at 273 K and 800 Torr) than that for CH_4, N_2 or H_2 (Fig. 3 and Table S6, ESI†). With 162.8 mg g^{-1} of the CO_2 uptake, **1a** is also comparable to many MOFs although its specific surface area is much lower (Table S5, ESI†). In general,

nitrogen-rich porous polymers have high CO_2 affinity and adsorption capacity due to dipole-quadrupole interactions between CO_2 and nitrogen sites. The obtained results demonstrate that the presence of high percentage of open nitrogen-donor sites within the framework is mainly responsible for the high and selective CO_2 uptake. The isosteric heat of adsorption (Q_{st}) for CO_2 was calculated based on the adsorption isotherms at different temperatures (273 and 298 K, Fig. S10, ESI†) through virial-equation. The CO_2 sorption isotherms are completely reversible, indicating that the interaction between CO_2 and **1a** is weak enough to allow material regeneration without heating. The Q_{st} at zero coverage was found to be 31.4 kJ mol^{-1}, and was followed by the convergence into a pseudo-plateau (~28.2 kJ mol^{-1}) with relatively high uptake (Fig. S11a, ESI†). It is within the desirable range for CO_2 sorbents according to recent findings by Wilmer *et al*.[5b] Remarkably, three consecutive cycles of CO_2 sorption isotherms at 298 K didn't show any hysteresis and exhibit very good reversibility even without further evacuation treatment after every cycle test (Fig.S11b, ESI†).

Table 1 CO_2 and N_2 uptake in selected MOFs at pressures relevant to post-combustion CO_2 capture.

MOFs	BET	CO_2 uptake at 0.15 bar (wt%, mmol g^{-1})	N_2 uptake at 0.75 bar (wt%, mmol g^{-1})	selectivity	Temp	Ref
mmen-Cu-BTTri	870	9.5/2.38	0.2/0.07	165[a] /327[b]	298	2a, 11
HKUST-1	1400	11.6/2.98	0.41/0.15	101	293	2a,12
en-Cu-BTTri	345	2.3/0.54	0.17/0.06	44	298	2a,17
Mg_2(dobdc)	2060	20.6/5.9	1.83/0.67	44	303	2a, 4
1a	701	2.69/0.63	0.22/0.08	40	298	This work
Fe-BTT	2010	5.3/1.27	0.95/0.34	18	298	2a, 23
Cu-BTTri	1900	2.9/0.69	0.49/0.18	19	298	2a,17
MOF-177	5400	0.6/0.14	0.39/0.14	5	298	2a,4

[a] reported by ref. 2a [b] reported by ref. 11

Since **1a** is stable in liquid water, the effect of water treatment (immersion in liquid water for 1 day) on the BET and CO_2 uptake were examined. The BET surface area decreased to about one quarter (from 701 to 179 m^2 g^{-1}) of the dehydrated form and the CO_2 uptake at 273 K decreased to about one third (from 82.8 to 30.4 cm^3 g^{-1}, see Fig. S12, ESI†) of its original value, which are attributed to the water adsorption in the channels. In combination with the PXRD analysis, the overall framework of **1a** remains intact upon exposure to water, indicating that the tetrazole-based linkers afford stronger M–N bond which protect the material from hydrolysis.

The CO_2/CH_4, CO_2/N_2, CO_2/H_2 selectivities at low pressure for **1a** were evaluated by using the initial slope ratios estimated from Henry's law[20,21] constants for single-component adsorption isotherms collected at 273 and 298 K as summarized in Fig. S13 and Table S7 (ESI†). Generally speaking, gas sorption on MOF's is most often driven by physisorption which is closely related to the specific surface area. Therefore, a high CO_2 uptake is often accompanied by a comparably high N_2 uptake as well. Remarkably, the selectivities of CO_2/N_2 and CO_2/H_2 at 273 K, which were calculated to be 69.7 and 577.2, respectively, are greatly higher than that of CO_2/CH_4 (13.3). Moreover, for all the cases, the selectivity decreases as temperature increases. The high adsorption selectivity of **1a** towards CO_2 over N_2 and H_2 under the same condition indicates that **1a** is highly applicable in the separation of CO_2 over N_2 and H_2.

The selectivity studies described above were also supported by results from the ideal adsorbed solution theory (IAST)[22] which were predicted based on the experimental single-component isotherms (Fig. S14 and Table S8–S9, ESI†). The CO_2/N_2 selectivity increases with decreasing total pressure and increasing P_{N_2} partial pressure (Fig. S15, ESI†). For the case of P_{CO_2} : P_{N_2}=0.15:0.75, which is a typical composition for the flue gas from power plants, the obtained CO_2/ N_2 selectivity of 40 (298 K) for **1a** at low pressure ranks among the high end for MOF materials (Table 1). In fact, only few materials show a high CO_2:N_2 selectivity (> 40), including the MOF-74 series, HKUST-1, and post-synthesis modified framework mmen-Cu-BTTri, bio-MOF-11, *etc*. The CO_2/H_2 selectivity increases with increasing P_{H_2} partial pressure (Fig. S16, ESI†). As for the CO_2 capture and H_2 purification under a 0.2:0.8 or a 0.4:0.6 CO_2/H_2 gas mixture, the selectivities at 298 K are in the range of 267–355 and 237–278, respectively.

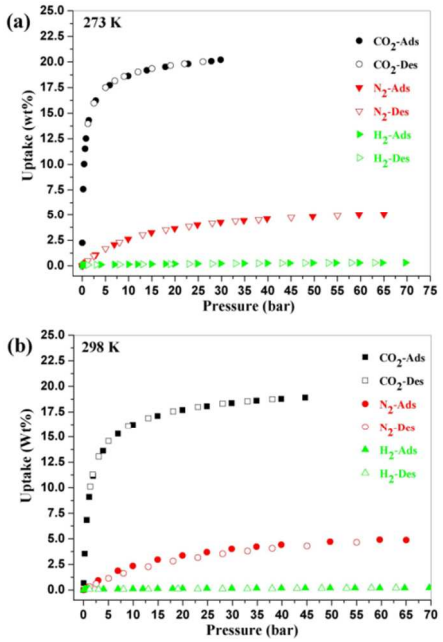

Fig. 4 High-pressure excess sorption isotherms of CO_2, H_2 and N_2 at 273 K (a) and 298 K (b) for **1a**.

Because the low pressure gas sorption studies indicate that **1a** is far from saturation at 1 bar, high pressure gas sorption measurements for CO_2, H_2 and N_2 were performed by using a MSB (Magnetic suspension balance) apparatus. The CO_2 uptake by **1a** shows a sharp increase below 5 bar. At saturation, **1a** takes up 253.44 mg g^{-1} of CO_2 at 273 K, 30 bar and 233.64 mg g^{-1} of CO_2 at 298 K, 45 bar (Fig. 4). As expected, **1a** can only adsorb a very small amount of N_2 (52.92 mg g^{-1}) and H_2 (2.84 mg g^{-1}) even at 273 K and 65 bar. The CO_2 uptake by **1a** is comparable to the reported values for Uio-66 (24.3 wt%, at 303 K and 18 bar)[24] and SNU-9 (29.9 wt%, at 298 K and 30 bar)[25] with a similar pore volume of 0.35 cm^3 g^{-1} for the former and 0.366 cm^3 g^{-1} for the latter. And, it is much lower than that of MOF-210 (74.2 wt% at 298 K and 50 bar)[26] and MOF-177 (56.8 wt% at 298 K and 30 bar)[27] with a very big pore volume of 3.60 and 1.89 cm^3 g^{-1}, respectively. These results further prove that CO_2 capacities at high pressure are much dependent on surface area and pore volume of the MOFs.

The CO_2 capture performance of **1a** under more practical condition was evaluated using a thermogravimetric analysis apparatus, with use of a CO_2–N_2 mixture (15:85 v/v) to simulate the major components of flue gas. About 30 mg sample of **1a** was blown repeatedly by CO_2–N_2 mixture and pure N_2 flow at 303 K (Fig. S17–

S18, ESI†). A weight change of ~0.8 wt% was observed at 2nd cycle and then a constant weight change of ~0.75 wt% was maintained in the following cycles (Table S10, ESI†), indicating that the material is able to withstand cyclic exposure to the mixed gas stream. Significantly, the material can be easily regenerated by switching the gas stream to N_2, which may render the material suitable for use as an adsorbent in pressure swing absorption type process for CO_2 capture.

Conclusions

In conclusion, through the incorporation of accessible nitrogen-rich tetrazole-based molecule of H_3BTT, we successfully isolated a water-stable poly-nuclear Cu(I)-based MOF which incorporates giant multi-prismatic cages interconnected by four types of windows. Extensive nitrogen-donor sites of 67% are exposed to these channels. The gas sorption studies toward CO_2, N_2, H_2 and CH_4 under low-pressure or high-pressure conditions are discussed in detail. These results indicate that the activated **1a** has high CO_2/N_2 and CO_2/H_2 sorption selectivities. Significantly, **1a** is able to maintain its CO_2 capacity after long-term storage under a more practical condition, which enables compound **1a** to serve as promising porous material for gas storage and separation. This work clearly demonstrates the potential of using the nitrogen-donor ligand for preparing porous inorganic materials use for selective capture of CO_2.

This work was financially supported by the NNSF of China (No. 21301152, 21371150), Foundation from the Priority Academic Program Development of Jiangsu Higher Education Institutions.

Notes and references

[a] *College of Chemistry and Chemical Engineering, Yangzhou University, Yangzhou, 225002, P. R. China. E-mail: bxdong@yzu.edu.cn (B-X. Dong); ylteng@yzu.edu.cn (Y-L. Teng). Fax: +86 51487975590-9201*

† Electronic Supplementary Information (ESI) available: Experimental details, characterization and additional structural data. CCDC 1034129. For ESI and crystallographic data in CIF or other electronic format see DOI: 10.1039/c000000x/

1 V. Nikulshina, C. Gebald, A. Steinfeld, *Chem. Eng. J.* 2009, **146**, 244.

2 (*a*) K. Sumida, D. L. Rogow, J. A. Mason, T.-M. McDonald, E. D. Bloch, Z. R. Herm, T. H. Bae, J. R. Long, *Chem. Rev*., 2012, **112**, 724; (*b*) R. Steeneveldt, B. Berger, T. A. Torp, *Chem. Eng. Res. Des*., 2006, **84**, 739.

3 Y.-F. Chen, J.-W. Jiang, *ChemSusChem*., 2010, **3**, 982.

4 Z. R. Herm, J. A. Swisher, B. Smit, R. Krishna, J. R. Long, *J. Am. Chem. Soc*., 2011, **133**, 5664.

5 *(a)* S. Keskin, T. M. V. Heest, D. S. Sholl, *ChemSusChem*., 2010, **3**, 879; *(b)* C. E. Wilmer, O. K. Farha, Y.-S. Bae, J. T. Hupp, R. Q. Snurr, *Energy Environ. Sci*., 2012, **5**, 9849; *(c)* A. Samanta, A. Zhao, G. K. H. Shimizu, P. Sarkar, R. Gupta, *Ind. Eng. Chem. Res*., 2012, **51**, 1438.

6 *(a)* J. Zhang, P. A. Webley, P. Xiao, *Energy Convers. Manage*., 2008, **49**, 346; *(b)* G. Li, P. Xiao, P. Webley, J. Zhang, R. Singh, M. Marshall, *Adsorption*, 2008, **14**, 415; *(c)* G. Li, P. Xiao, P. Webley, J. Zhang, R. Singh, *Energy Procedia.,* 2009, **1**, 1123.

7 *(a)* C. F. Martin, M. G. Plaza, J. J. Pis, F. Rubiera, C. Pevida, T. A. Centeno, *Sep. Purif. Technol*., 2010, **74**, 225; *(b)* J. Silvestre-Albero, A. Wahby, A. Sepúlveda-Escribano, M. Martínez-Escandell, K. Kaneko, F. Rodríguez-Reinoso, *Chem. Commun*., 2011, **47**, 6840; *(c)* M. G. Plaza, S. García, F. Rubiera, J. J. Pis, C. Pevida, *Chem. Eng. J*., 2010, **163**, 41.

8 *(a)* 2014 metal-organic frameworks issue. *Chem. Soc. Rev*., 2014, **43**, 5415–6172; *(b)* H. Furukawa, K. E. Cordova, M. O'Keeffe, O. M. Yaghi, *Science*, 2013, **341**, 1230444.

9 R. Babarao, J.-W. Jiang, *J. Am. Chem. Soc*., 2009, **131**, 11417.

10 P. Nugent, Y. Belmabkhout, S. D. Burd, A. J. Cairns, R. Luebke, K. Forrest, T. Pham, S. Q. Ma, B. Space, L, Wojtas, M. Eddaoudi, M. J. Zaworotko, *Nature*, 2013, **495**, 80.

11 T. M. McDonald, D. M. D'Alessandro, R. Krishna, J. R. Long, *Chem. Sci*., 2011, **2**, 2022.

12 P. Aprea, D. Caputo, N. Gargiulo, F. Iucolano, F. J. Pepe, *Chem. Eng. Data*., 2010, **55**, 3655.

13 Y. S. Bae, O. K. Farha, J. T. Hupp, R. Q. Snurr, *J. Mater. Chem*., 2009, **19**, 2131.

14 P. Nugent, V. L. Rhodus, T. Pham, K. Forrest, L. Wojtas, B. Space, M. J. Zaworotko, *J. Am. Chem. Soc*., 2013, **135**, 10950.

15 *(a)* Q.-Y. Yang, C.-L. Zhong, *J. Phys. Chem. B*., 2006, **110**, 17776; *(b)* D. Wu, Q. Xu, D.-H. Liu, C.-L. Zhong, *J. Phys. Chem. C*., 2010, **114**, 16611.

16 *(a)* Q.-P. Lin, T. Wu, S.-T. Zheng, X.-H. Bu, P.-Y. Feng, *J. Am. Chem. Soc*., 2012, **134**, 784; *(b)* X. Zhu, S. M. Mahurin, S. H. An, C. L. Do-Thanh, C.-C. Tian, Y.-K. Li, L. W. Gill, E. W. Hagaman, Z. J. Bian, J.-H. Zhou, J. Hu, H.-L. Liu, S. Dai, *Chem. Commun*., 2014, **50**, 7933.

17 A. Demessence, D. M. D'Alessandro, M. L. Foo, J. R. Long, *J. Am. Chem. Soc*., 2009, **131**, 8784.

18 X.-J. Wang, P.-Z. Li, Y.-F. Chen, Q. Zhang, H.-C. Zhang, X.-X. Chan, R. Ganguly, Y.-X. Li, J.-W. Jiang, Y.-L. Zhao, *Sci Rep*., 2013, **3**, 1149.

19 A. L. Spek, *J. Appl. Crystallogr*., 2003, **36**, 7.

20 J. A. Mason, K. Sumida, Z. R. Herm, R. Krishna, J. R. Long, *Energy Environ. Sci*., 2011, **4**, 3030.

21 *(a)* A. K. Sekizkardes, T. slamoğlu, Z. Kahveci, H. M. El-Kaderi, *J.Mater. Chem. A*., 2014, **2**, 12492; *(b)* M.-X. Zhang, Q. Wang, Z.-Y. Lu, H.-Y. Liu, W.-L. Liu, J.-F. Bai, *CrystEngComm*., 2014, **16**, 6287.

22 *(a)* A. L. Myers, J. M. Prausnitz, *AIChE J.* 1965, **11**, 121; *(b)* Y. S. Bae, K. L. Mulfort, H. Frost, P. Ryan, S. Punnathanam, L. J. Broadbelt, J. T. Hupp, R. Q. Snurr, *Langmuir*, 2008, **24**, 8592; *(c)* B. Mu, F. Li, K. S. Walton, *Chem. Commun*., 2009, **18**, 2493.

23 K. Sumida, S. Horike, S. S. Kaye, Z. R. Herm, W. L. Queen, C. M. Brown, F. Grandjean, G. J. Long, A. Dailly, J. R. Long, *Chem. Sci.,* 2010, **1**, 184.

24 A. D. Weirsum, E. Soubeyrand-Lenoir, Q.-Y. Yang, B. Moulin, V. Guillerm, M. B. Yahia, S. Bourrelly, A. Vimont, S. Miller, C. Vagner, M. Daturi, C. Guillaume, C. Serre, G. Maurin, P. L. Llewellyn, *Chem.—Asian J*., 2011, **6**, 3270.

25 H. J. Park, M. P. Suh, *Chem. Commun*., 2010, **46**, 610.

26 H. Furukawa, N. Ko, Y. B. Go, N. Aratani, S. B. Choi, E. Choi, A. O. Yazaydin, R. Q. Snurr, M. O'Keefe, J. Kim, O. M. Yaghi, *Science,* 2010, **329**, 424.

27 D.-W. Jung, D.-A. Yang, J. Kim, J. Kim, W.-S. Ahn, *Dalton Trans*., 2010, **39**, 2883.

